ACS Photonics

pubs.acs.org/journal/apchd5

Article

Efficient Modeling and Tailoring of Nonlinear Wavefronts in Dielectric Metasurfaces

David Hähnel, Jens Förstner,* and Viktor Myroshnychenko*

Cite This: https://doi.org/10.1021/acsphotonics.2c01967

Read Online

ACCESS | Metrics & More | Article Recommendations | Supporting Information

ABSTRACT: Dielectric metasurfaces provide a unique platform for efficient harmonic generation and optical wavefront manipulation at the nanoscale. Tailoring phase and amplitude of a nonlinearly generated wave with a high emission efficiency using resonance-based metasurfaces is a challenging task that often requires state-of-the-art numerical methods. Here, we propose a simple yet effective approach combining a sampling method with a Monte Carlo approach to design the third-harmonic wavefront generated by all-dielectric metasurfaces composed of elliptical silicon nanodisks. Using this approach, we theoretically demonstrate the full nonlinear 2π phase control with a uniform and highest possible amplitude in the considered parameter space, allowing us to design metasurfaces operating as third harmonic beam deflectors capable of steering light into a desired direction with high emission efficiency. The TH beam deflection with a record calculated average conversion efficiency of 1.2×10^{-1} W^{-2} is achieved. We anticipate that the proposed approach will be widely applied as alternative to commonly used optimization algorithms with higher complexity and implementation effort for the design of metasurfaces with other holographic functionalities.

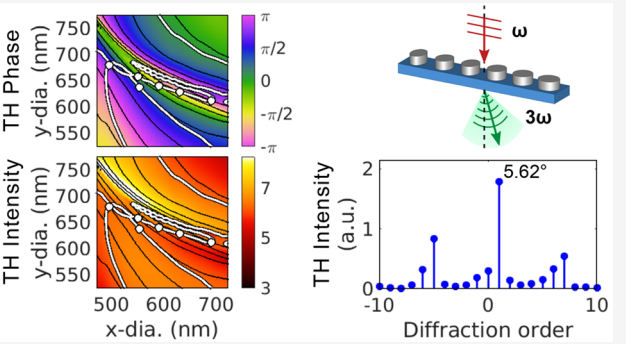

KEYWORDS: *nonlinear optics, dielectric metasurfaces, third-harmonic generation, nonlinear wavefront control, nonlinear beam steering*

INTRODUCTION

Artificially designed metasurfaces comprising a spatial arrangement of planar arrays of subwavelength resonators have recently attracted tremendous scientific and technological attention, as they exhibit a number of extraordinary properties including the ability for complex optical wavefront engineering.[1−5] These ultrathin structures permit to control and manipulate the amplitude, phase, direction, and polarization state of the incident light along the surface at the subwavelength scale, opening a new avenue within the dynamic field of nanophotonics and nanooptics. This makes them promising candidates in a wide range of exciting devices ranging from polarization converters[6−8] and optical sensors[9,10] to flat lenses[11,12] and complex holograms.[13−16]

The wavefront control is commonly achieved by using geometric-phase (Pancharatnam-Berry phase) metasurfaces[16−19] or resonant (Huygens) metasurfaces.[20−23] In the former case, the wavefront is modulated by locally positioning and rotating the resonators in a certain way on the surface, whereas in the latter case it is realized by varying size and shape of the individual resonators that, in turn, control the excitation of a variety of optical resonances locally hosted within them. Huygens metasurfaces usually exhibit higher conversion efficiency and can operate under the excitation with linearly polarized light. In this context, metasurfaces made of high-index dielectric resonators have gained great popularity in recent years as an alternative to their metallic counterparts, as they possess crucial advantages and offer more degrees of freedom in the wavefront design. First, the dielectric resonators exhibit very low dissipation loss and thus have a high laser-damage threshold. Second, they are capable of hosting electric and magnetic multipolar resonances that can be spectrally tailored to overlap and even swap positions in the spectrum, while in common metallic nanoparticles only electric resonances are fully supported[24] due to their weak magnetic response within the optical range.[25] Furthermore, the richness of these resonances can lead to the excitation of nonradiative modes and ultrasharp Fano resonances in these structures. Finally, in contrast to metallic nanoparticles, whose localized surface plasmon resonances are confined at the metal−dielectric interface,[24] the Mie modes of high-index dielectric resonators are accommodated inside the whole volume, increasing the excitable, optical mode volume.[26] All these

Received: December 15, 2022

advantages make dielectric metasurfaces appealing candidates for efficient nonlinear light generation.[27−29] A variety of exciting functionalities in the nonlinear domain have recently been shown, including nonlinear imaging,[30−32] beam steering,[19,23] and ultrafast optical modulation.[33] In particular, the designed nonlinear metasurfaces made of silicon, germanium, or aluminum gallium arsenide nanoparticles have demonstrated large enhancement of the conversion efficiency and possibility for advanced nonlinear wavefront control.[34−37]

Many existing papers are aimed at either an amplitude amplification or phase control of the harmonic signal; however, there is a lack of publications on full nonlinear wavefront control, which is a challenging task, especially when considering the tailoring of the continuous phase in a certain range at constant and preferentially maximal amplitude using resonance-based metasurfaces. These challenges arise mainly from the narrow-band behavior of the high-order electric and magnetic resonances and couplings between them which are strongly influenced by the geometrical parameters of the resonators.[23] This implies that small changes in the geometrical parameters of the resonators can result in large conversion efficiency jumps and large phase variations, making such metasurfaces sensitive to fabrication imperfections. The problem is compounded by the fact that generated nonlinear radiation depends strongly on variations of the phase and amplitude of the fields not only at pump frequency but also at high harmonic frequency. Furthermore, to achieve above-mentioned functionalities, the resonators are usually packed in arrays whose collective responses have to be taken into account as well. All of the above-mentioned factors require sophisticated optimization for the precise determination of the proper set of resonators. For this purpose, different methods have been extensively applied, such as the gradient descent method,[23,38] topology optimization,[39−41] and the evolutionary optimization technique,[42,43] in conjunction with electro-magnetic solvers like the finite-difference time-domain method, finite integration technique, etc. Besides, different machine learning techniques and deep neural network-based approaches have been increasingly considered recently to further accelerate the metasurface design process.[44−46]

In this work, we propose a simple and robust sampling method in conjunction with Monte Carlo (MC) simulation to design and optimize a nonlinear wavefront of Huygens all-dielectric metasurfaces. We demonstrate our approach for a classical metasurface composed of elliptical nanodisk resonators made of silicon that generate a third-harmonic (TH) radiation under external illumination, placed on a silicon dioxide substrate. Information about the nonlinear phase and amplitude are locally encoded through an adjustment of the lateral dimensions of nanodisks. A MC simulation is employed to explore a geometrical parameter space and find optima with enhanced conversion efficiency. The sampling method is then applied to select a collection of resonators generating a TH field with a phase discretely spanning the full 2π range at the uniform and highest possible amplitude in the considered parameter space. We show the power of our approach by designing and optimizing dielectric metasurfaces that act as nonlinear beam deflectors. The high amplification of TH generation emitted along the prescribed angle is achieved in theory. Our combined approach clearly demonstrates the possibility of designing and optimizing nonlinear Huygens metasurfaces with a variety of functionalities without the use of sophisticated optimization methods.

RESULTS AND DISCUSSION

Model of the Metasurface for Nonlinear Beam Deflection. To implement our approach, we utilize a metasurface composed of a set of silicon elliptical cylinder disks placed on a silicon dioxide substrate.[23] It exhibits TH generation under external illumination since silicon belongs to the group of centrosymmetric materials with a significant third-order nonlinearity. We aim to design a metasurface that produces a TH beam deflection into a desired direction (metadeflector), as illustrated in Figure 1a. The deflection of

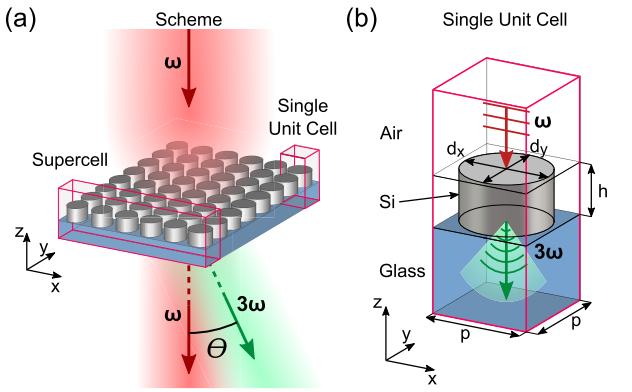

Figure 1. (a) Schematic view of a dielectric metasurface for nonlinear beam deflection. The metasurface is composed of an array of supercells each of which consists of N silicon resonators in a form of elliptical cylinders with different lateral dimensions placed on a SiO_2 substrate (blue block). The metasurface is illuminated from the top by linear x-polarized light at the fundamental frequency ω (red arrow) and deflects the TH wave 3ω (green arrow) into the substrate by the angle θ. The incident and generated TH waves experience a 2π phase shift over the length of each supercell. (b) A model of a periodic square unit cell used in the design and optimization. Phase and amplitude control of the TH field is achieved by tailoring the resonance condition of the Si resonator through variation of the cell periodicity p, resonator height h, and elliptical base diameters d_x and d_y.

the TH output wave is caused by a stepwise linear phase shift along the surface induced by the dielectric resonators. Such a metasurface is composed of a periodic array of supercells, each of which consists of a set of resonators emitting nonlinear fields with a linear phase profile spanning the full $0-2\pi$ range. Additionally, we pursue maximization of the nonlinear emission efficiency with a uniform amplitude for all resonators. The TH steering angle θ for such a supercell can be calculated as $\theta = \sin^{-1}(\lambda_{TH}/Np)$, where λ_{TH} is the TH wavelength in the output medium, N is the number of resonators in the supercell, and p is the dimension of the single unit cell. The periodic properties of such metasurfaces can be exploited to reduce the model in the simulations to one supercell, i.e., a single line of resonators schematically depicted in Figure 1a, with the application of periodic boundary conditions. The overall response of such a supercell is assumed to depend only on the properties of the individual resonators. Therefore, in order to minimize memory space and time consumption required for the design and optimization process, in a first step we can further reduce the simulation model to a unit cell with a single resonator from the entire structure, as shown in Figure 1b. In this case, the main assumption exploited is that the coupling between resonators of different shape is comparable to equal shapes thus not affecting the TH far-field much. The validity of

https://doi.org/10.1021/acsphotonics.2c01967
ACS Photonics XXXX, XXX, XXX−XXX

this assumption will be discussed later.[47] The phase and amplitude of the nonlinear beam can be controlled by varying the geometrical parameters such as the square unit cell size p, the resonator height h and elliptical base diameters d_x, d_y. Calculations of the linear and nonlinear electromagnetic fields were performed by employing the finite element method-based COMSOL Multiphysics.[48] Details of the numerical simulations are provided in the Methods section. Finally, we note that this work is mainly focused on the design of the metasurfaces with a full-phase control of the high efficiency harmonic field and does not explore the origin and nature of electromagnetic resonances inducing TH emission.

Sampling Method for the Design of the TH Phase and Amplitude. The work of Wang et al.[23] was used as a starting point, providing us with a preoptimized set of parameters for the nonlinear silicon metadeflector. For the design of our initial metasurface, we also use a pump wavelength of 1615 nm, a lattice periodicity of 550 nm, a nanodisk height of 617 nm, and elliptical base diameters in the range from 320 to 535 nm. To achieve the desired nonlinear beam steering, the phase and amplitude information for each nanodisk in the supercell at the TH wavelength (538.3 nm) is required. For this purpose, we computed maps which relate a given TH phase and amplitude to the values of elliptical basis diameters d_x and d_y, as illustrated in Figure 2c,d.[49] Additionally,

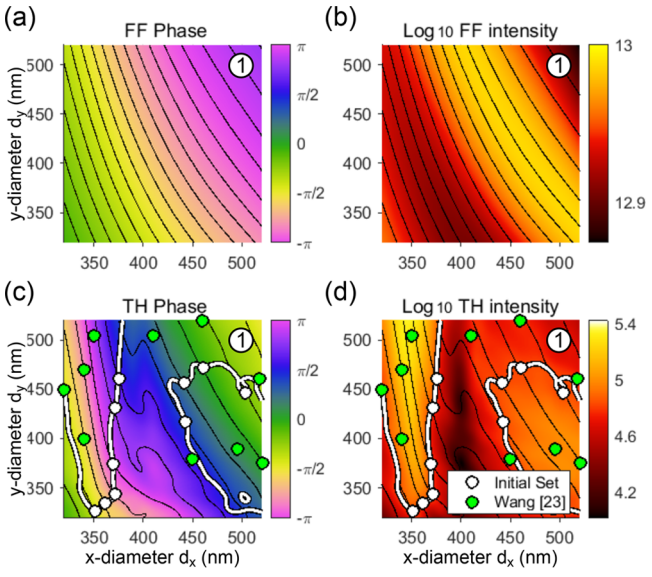

Figure 2. Sampling method for the design of nonlinear metasurfaces with full nonlinear phase and amplitude control. (a) Phase and (b) intensity maps of the FF electric field at λ = 1615 nm in transmission direction as a function of nanodisk elliptical diameters d_x and d_y. The periodicity of the unit cell and the nanodisk height are fixed at p = 550 nm and h = 617 nm, respectively. Black curves correspond to the contour isolines of the phase angles along which the function has constant values. (c) Phase and (d) intensity maps of the TH electric field at λ = 538.3 nm with contour isolines. The values of the phase contour isolines (black curves) are equidistantly distributed in $2\pi/10$ steps. The white curves in (c) and (d) represent the contour isolines for the highest intensity value that continuously covers the full phase angle range of 2π in the phase map (c). Ten nanodisks with elliptical diameters d_x and d_y marked by the white dots are selected using a sampling method based on the detection of a predefined number of intersections between phase and intensity contours. The green dots indicate the nanodisks optimized by a gradient descent method in the work of Wang et al.[23]

the contour isolines of the TH phase angles along which the function has constant values (black curves) are added. The values of the phase contours are equidistantly distributed in the $0-2\pi$ range determining also the number of distinct resonator geometries. The phase map calculated in this parameter range clearly covers a full 2π relative phase shift. Taking inspiration from a sampling method proposed by Almeida et al. for design of phase-only plasmonic holograms in the nonlinear domain,[13] we select a set of ten resonators required to construct a similar metadeflector as in ref 23. This is done by detecting a predefined number of intersections (white dots) between phase contours (black curves) and amplitude contour at the highest possible uniform amplitude (white curve), which covers the full phase angle range of $0-2\pi$, as shown in the maps of Figure 2c,d. This selection procedure makes the method very simple, adaptive, and robust to any number of resonators and any phase and amplitude profiles required. Interestingly, in contrast to the nanodisks optimized by the gradient descent method in the work of Wang et al. demonstrating varying harmonic amplitudes (green dots), the nanodisks selected by the sampling method have a perfectly uniform amplitude and, importantly, a similar magnitude as the average amplitude among the nanodisks in the referenced work.[23] The phase and amplitude maps at FF together with contour isolines of the phases are also shown for comparison in Figure 2a and b, respectively. The smooth change of the linear phase and amplitude suggests detuning from the resonance peaks of nanodisks in this parameter range. On other side, the absence of close correlations between the phase and amplitude maps at FF and TH, manifested in the smooth and highly distorted profiles of the phases and amplitudes at FF and TH, respectively, confirms the strong impact of Mie resonances at the harmonic frequency.

Monte Carlo Simulation for TH Amplitude Enhancement. Aiming to further increase the intensity of the TH radiation, we employ a Monte Carlo simulation that permits us to explore the full parameter space and find promising geometrical parameters furnishing the enhanced TH signal. It is very simple in implementation and uses the random sampling to probe the four-dimensional (4D) parameter space with smaller number of sampled points for the same field prospect compared to the computationally time-consuming uniform grid sampling. This optimization approach in combination with the sampling method introduces an exploration dynamics into the design process which is typically not addressed by standard optimization algorithms. In particular, the Monte Carlo method thoroughly explores the parameter space and provides rich information about the system behavior and tendencies. Furthermore, it offers capabilities to dynamically increase the resolution of the system and even the area of exploration by adding more sampling points posterior. The procedure consists of the following steps. First, we pick out four geometric parameters affecting the TH intensity, namely, the lattice periodicity, the nanodisk height, and two elliptical base diameters. In the spirit of MC simulations, the values of these parameters are randomly generated in defined parameter ranges, and the TH intensity of this single "random" resonator in the periodic unit cell is calculated as explained in the Methods section. The lattice periodicity is chosen to be in the range from 430 to 1070 nm, and the nanodisk height is in the range from 160 to 740 nm, whereas the allowed elliptical diameters depend on the lattice periodicity. Specifically, the minimal diameter is 35%

https://doi.org/10.1021/acsphotonics.2c01967
ACS Photonics XXXX, XXX, XXX−XXX

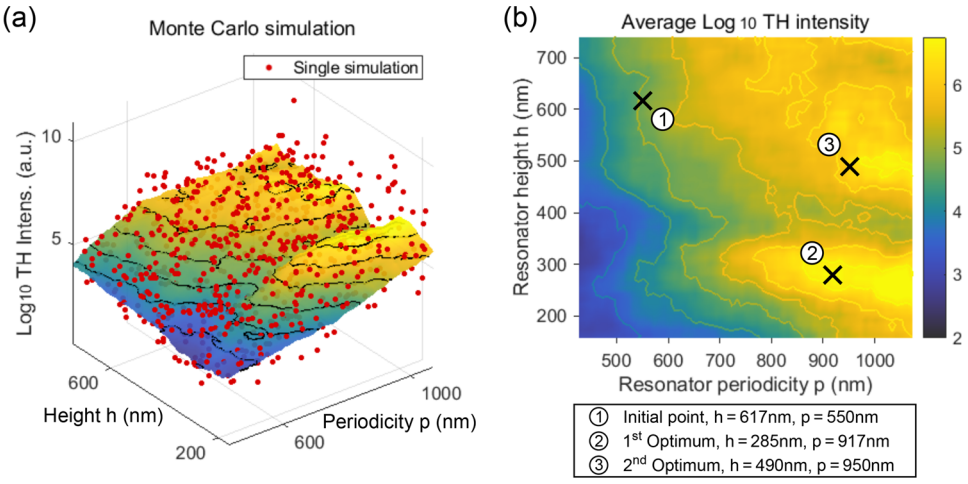

Figure 3. Monte Carlo simulation for optimization of metasurfaces with enhanced TH generation. (a) Scatter plot of TH intensity in transmission direction (red dots) calculated as a function of four geometrical parameters, the lattice periodicity, nanodisk height, and the two elliptical base diameters. The values of these parameters are randomly generated in the defined parameter ranges for a large collection of samples. The surface plot represents the averaged TH intensity (log scale) calculated by applying a 2D moving average procedure to the scattered data and plotted as a function of the lattice periodicity and nanodisk height. (b) Projection of the surface plot in (a) on the plane, showing regions of high intensity. Three black crosses in the map indicate parameter sets for the lattice periodicity and nanodisk height selected for design of metadeflectors: initial set 1 demonstrated in Figure 2 (p = 550 nm, h = 617 nm), optimum set 2 (p = 917 nm, h = 285 nm), and optimum set 3 (p = 950 nm, h = 490 nm).

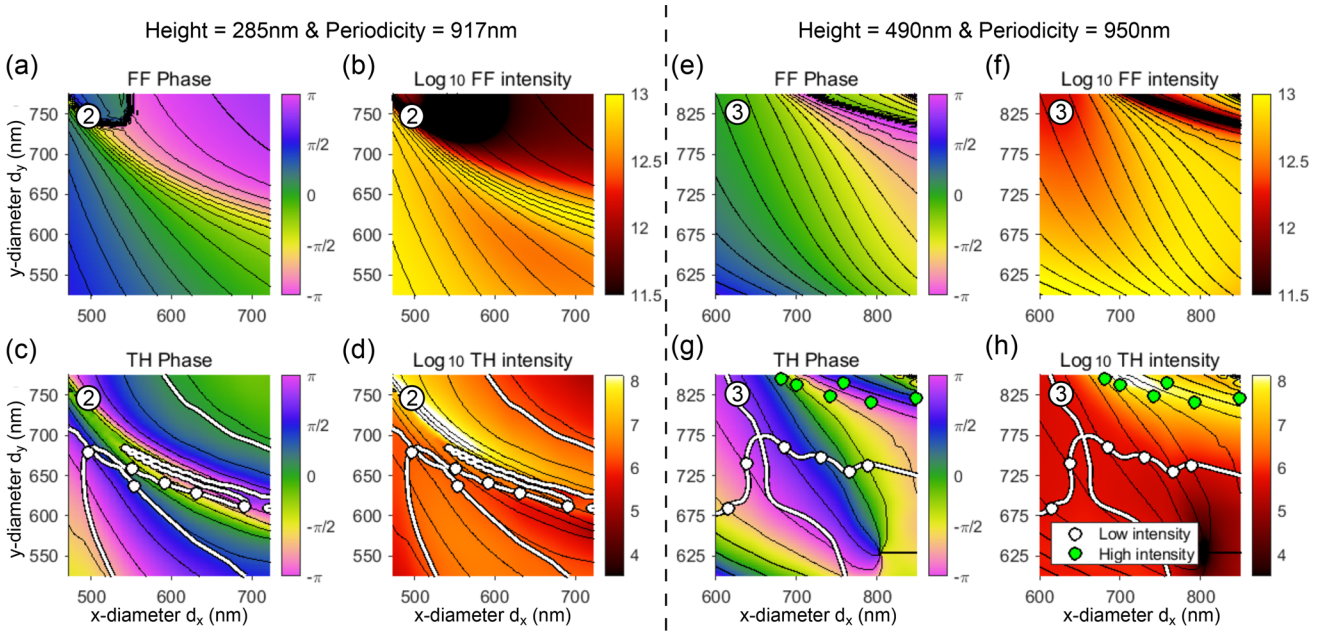

Figure 4. Sampling method for the design of the nonlinear metasurfaces with the MC-optimized amplitude. (a−d) Phase and intensity maps of the electric field in transmission direction at (a, b) FF and (c, d) TH for optimum set 2 with p = 917 nm and h = 285 nm, optimized by a MC procedure in Figure 3b. Black curves in maps correspond to the equidistantly distributed contour isolines of the phase angles along which the function has constant values. White curves in (c, d) represent the contour for the highest TH intensity value that covers the full 2π phase range in the phase map (c). Six individual nanodisks marked by the white dots are selected using a sampling method. (e−h) Same as in (a)−(d) for optimum set 3 corresponding to the periodicity p = 950 nm and the nanodisk height h = 490 nm. Two sets of nanodisks are selected using a sampling method (white dots) and manually in a region of a significantly higher intensity (green dots).

of the lattice periodicity, and the maximal diameter always assures a 90 nm gap between neighboring nanodisks, i.e., $0.35p \leq d_x, d_y \leq p - 90$ nm. The upper bounds for the periodicity and nanodisks height are limited due to the high memory and computational costs. Although, the scanned ranges cover the respective parameter values used in the majority of work published on Si-based metasurfaces. Furthermore, exploring larger periodicity would eventually lead to significant TH radiation into the higher diffraction orders. The lower bound for the gap between nanodisks of 90 nm also reduces the computational cost and allows to avoid fabrication tolerance problems. The large collection of such samples, ∼24000, was generated in order to accurately detect regions of high intensity in a 4D parameter space. Figure 3a illustrates the resulting scatter plot of TH intensity (red dots) as a function of the lattice periodicity and nanodisk height by projection, disregarding the actual values of elliptical base diameters. Note that only a small part of dense scattered data are plotted

https://doi.org/10.1021/acsphotonics.2c01967
ACS Photonics XXXX, XXX, XXX−XXX

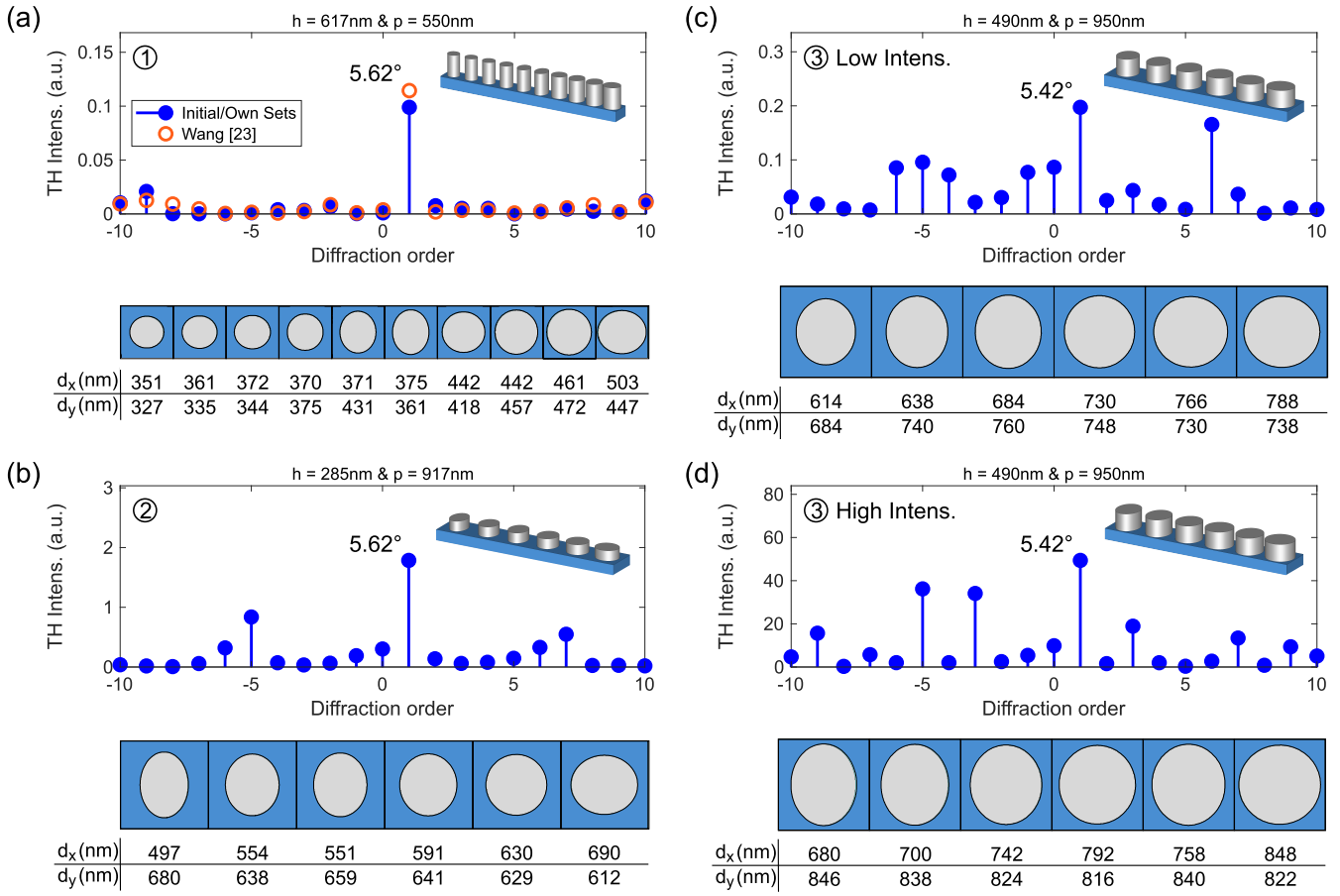

Figure 5. Metasurfaces for nonlinear beam deflection. (a–d) Discrete diffraction spectra of TH field in forward direction for four designed metasurfaces operating as beam deflectors: (a) initial set 1, (b) optimum set 2, (c) optimum set 3 of low intensity, and (d) optimum set 3 of high intensity. The intensity is given in arbitrary units. The angle of the first diffraction order is indicated in each spectrum for guidance. The corresponding supercell of the structure and lateral dimensions of the nanodisks used in the simulations are shown in each panel. Orange circles in (a) represent the discrete diffraction spectra of TH field for a metasurface optimized by a gradient descent method in the work of Wang et al.[23]

for better visibility. Next, these intermediate results are processed by applying a 2D moving average procedure to the scattered data points and calculating the averaged TH intensity as a function of the lattice periodicity and resonator height. The "moving" window has a size of 45 nm × 45 nm and is shifted with a step size of 10 nm. The resulting surface plot of average TH intensity presented in Figure 3a unveils tendencies in the parameter space. The projection of the surface plot on the plane represented in Figure 3b indicates several distinguishable maxima with considerable high intensities. Finally, the lattice periodicity and resonator height which resulted in highest average TH intensity can be selected in this map, reducing the parameter set to two nanodisk diameters used for final manipulation of the TH phase and amplitude. The highest maximum in the map, marked by a black cross and named as optimum set 2, corresponds roughly to the lattice periodicity of 917 nm and a nanodisk height of 285 nm. We also select another prominent maximum, optimum set 3, with the periodicity of 950 nm and nanodisk height of 490 nm. The other maxima located at the higher values of parameters are neglected in order to consider fabrication restrictions and to avoid higher-order diffraction. The initial geometry optimized by Wang et al.[23] and explored in Figure 2 (p = 550 nm, h = 617 nm) is also marked in the map as the initial set 1. Importantly, the comparison of initial and optimum sets indicates the increase of average TH intensity by approximately two orders. Note that this is solely the average amplification of the radiated TH intensity from the homogeneous metasurface.

Design of MC-Optimized Metadeflectors. Having two sets of optimal parameters for the lattice periodicity and nanodisk height gained from the MC optimization procedure (optimum sets 2 and 3 in Figure 3), we computed the corresponding linear and TH phase and intensity maps by sweeping across the elliptical diameters of the nanodisk, as presented in Figure 4. For each case, the sampling method presented above was applied to select a set of resonators (white dots) spanning the phase of 0–2π range with equal spacing and the highest possible uniform amplitude (white curves). Noting the significant differences in the values of the initial and optimum lattice periodicities and aiming at nearly the same deflection angle for the TH beam, we selected six nanodisks featuring approximately the same supercell length as initial set 1 with 10 resonators explored in Figure 2. A close look at the TH phase map for optimum set 2 shown in Figure 4c reveals an abrupt change of the phase along the winding amplitude contour (white curves) caused mainly by the overlap of the excited optical resonances. This implies a small variation in some selected nanodisk diameters (along the y-axis) and, thus, requires high fabrication accuracy. In contrast, for optimum set 3 (Figure 4g,h), the phase changes smoothly along the amplitude contour (white curves), resulting in a high difference

https://doi.org/10.1021/acsphotonics.2c01967
ACS Photonics XXXX, XXX, XXX–XXX

in the selected nanodisk diameters, but the TH intensity decreases by 1 order of magnitude compared to the one for optimum set 2. Pursuing further the high TH radiation, we focus our attention on a resonant area of high intensity in the upper right corner of Figure 4h. This TH enhancement is caused by a strong resonance feature at FF manifested in Figure 4f (black area in the upper-right corner). There is no perfectly uniform amplitude contour spanning the 2π phase range in this region. However, by relaxing the uniform amplitude condition, the set of six required resonators possessing a nearly uniform TH intensity with 2π phase coverage can be manually selected, as marked by green dots. It is named optimum set 3 of high intensity. In summary, the TH intensity amplification by a factor ∼30 (optimum set 2), ∼7 (optimum set 3, low intensity), and ∼1000 (optimum set 3, high intensity) with respect to the reference intensity (initial set 1) is achieved by employing MC simulation for optimization.

TH Beam Steering. To prove the ability of TH light steering by engineering the $0-2\pi$ phase wavefront using an all-dielectric metasurface, we modeled four metadeflectors using the geometrical parameters designed in the previous sections. All supercells generate a $0-2\pi$ linear phase gradient at the TH wavelength over approximately the same overall supercell length producing a global deflection of the output wave by an angle θ. To estimate the directionality of the TH emission, we calculated discrete diffraction spectra by employing near-field to far-field transformation (NFFFT) for periodic structures,[50] as presented in Figure 5. The corresponding model of the supercell together with the geometry of individual nanodisks and calculated angular value of the first diffraction order are also indicated for each case. As expected, all metasurfaces produce the TH radiation mainly into the positive first diffraction order +1 at an angle around 5.6° relative to the direction of incident light. These angles differ to some degree owing to slightly distinct lengths of the supercells. Remarkably, the intensities of TH emitted into the first diffraction order for our initial supercell 1 and supercell optimized in the work of Wang et al.[23] have a similar magnitude, as shown in Figure 5a. Furthermore, the TH efficiencies of all MC-optimized supercells (Figure 5b−d) are larger than that of the initial supercell 1. In particular, the metadeflectors optimized using the MC procedure in combination with the sampling method shown in Figure 5b,c demonstrate amplification of the TH intensity by a factor of ∼20 and ∼2, respectively. Moreover, the supercell optimized using MC simulation in conjunction with the manual selection of resonators (Figure 5d) reveals even larger amplification of the TH intensity by a factor of ∼500. Such high enhancement is achieved due to the selection of appropriate resonators for the supercell in a region near a strong high-order optical resonance at the fundamental frequency as can be seen in the upper-right corner of Figure 4f (see also Figure S1 of Supporting Information). Finally, we quantitatively estimate the TH normalized conversion efficiencies of the initial (Figure 5a) and most efficient MC-optimized (Figure 5d) supercells. We attained a TH beam deflection into the desired channel with peak power-independent conversion efficiencies $\left(\eta_{t,\mathrm{sim}} = P_{\mathrm{TH,sim}}/P^3_{\mathrm{in,sim}}\right)$ of 9.3×10^{-12} W^{-2} and 1.7×10^{-9} W^{-2}, respectively.

Aside from the conversion efficiency of the beam deflectors, a few words should be added about the diffraction efficiency into the first diffraction order that varies greatly among the models. The diffraction spectra for the initial and MC-optimized metadeflectors shown in Figure 5a,b exhibit a high diffraction efficiency in which almost all diffraction orders are well damped except for the +1 order. For the remaining two models shown in Figure 5c,d, other undesirable diffraction orders notably appear in the diffraction spectra. These directionality diagrams are influenced by an interplay of a number of factors and assumptions present in our approach. First, although our optimization of the TH field generated by the single unit cell comprises coupling between identical neighboring resonators, it ignores the difference in coupling strengths induced by the interaction between neighboring resonators with different dimensions and thus resonances in the supercell. Especially, the coupling strength significantly depends on either the selected resonators operate in an off- or on-resonant state at the fundamental frequency, with the effect being much stronger for the latter. Therefore, only if the neighboring shapes and gaps of nanodisks do not differ much, specifically if the nanodisk shapes and gaps smoothly change within the supercell, the presence of nonidentical near-neighbors does not alter the wavefront of the unit cell much. Second, the subwavelength periodicity of the single unit cell at the TH wavelength is essential in order to avoid significant radiation into the higher diffraction orders. Finally, the theoretical maximum of diffraction efficiency is limited by the number of discrete phase steps, in such a manner that it falls as the number of resonators in the supercell decreases.[51]

Indeed, the initial supercell composed of ten nanodisks with the smallest lattice period (550 nm) and detunded from the resonance peaks (Figure 5a) reveals the best diffraction efficiency. Interestingly, the supercell shown in Figure 5b consisting of six detuned resonators with a larger periodicity of 917 nm also demonstrates a quite high diffraction efficiency, mainly due to the large gaps between the neighboring nanodisks. For both supercells, the excited electric fields inside all nanodisks have similar profiles, as shown in Figure S2a,b of the Supporting Information, leading to the uniform radiation of the TH field from the individual resonators. On the other hand, the worst accuracy is observed for the supercells composed of six nanodisks with the largest lattice periodicity (950 nm), small gaps between the resonators, and exhibiting the strong resonant nature at FF (Figure 5c,d). These factors result in an enhanced near-field interaction with varying coupling strength among the nonidentical nanodisks and, consequently, the strong distortion of the near-field profiles inside the resonators. Indeed, Figure S2c,d of the Supporting Information demonstrates highly nonuniform near-fields in all nanodisks of the metadeflectors attributed possibly to the enhanced symmetry breaking and thus excitation of additional antisymmetric modes inside the nanodisks (due to the interaction between adjacent nanodisks of different diameters) as well as the enhanced shadowing-like effect around the left and right sides of the 2π phase jump, i.e., at the location of neighboring the smallest and largest nanodisks. This strongly violates the translational invariance assumed by the phase and amplitude maps computation and leads to undesirable nonuniform radiation of the TH field from the individual nanodisks in the supercell, that, eventually, significantly reduces the diffraction efficiency.[47] Nevertheless, the high conversion efficiency of the beam deflectors is our primary goal in this optimization rather than a high level of diffraction efficiency that can be improved inside the presented approach, for instance, by adding an additional optimization goal to the

https://doi.org/10.1021/acsphotonics.2c01967
ACS Photonics XXXX, XXX, XXX−XXX

present scheme which minimizes the overall TH emission into nonzero diffraction orders for a periodic unit cell with a single resonator.

Yet, it is worthy to compare our numerical results with experimentally obtained values provided in the reference work of Wang et al.[23] In that experiment, for the average Gaussian pump power of 200 mW, a pulse length of 300 fs, a repetition rate of 20 MHz, and a diffraction-limited focusing (NA = 0.1, 4×), the measured TH peak power-independent conversion efficiency is $\eta_{av,exp} = 1.4 \times 10^{-4}$ W^{-2}, respectively, which is a common value for wavefront shaping metasurfaces reported in previous works.[29,49] We adopted our numerically calculated values to the parameters and conditions used in the experiment, as described in Section S3 of the Supporting Information. We calculated nearly the same averaged conversion efficiency for our initial supercell, i.e., $\eta_{av,sim} = 2.1 \times 10^{-4}$ W^{-2}, while for the MC-optimized supercell the corresponding value is $\eta_{av,sim} = 1.2 \times 10^{-1}$ W^{-2}. The latter is, to the best of our knowledge, three orders of magnitude higher than the record value for THG in Mie-resonant silicon metasurfaces reported so far.[31] Overall, these results demonstrate that our combined approach can be successfully used for design and optimization of nonlinear metasurfaces. Although the approach requires a large amount of calculated data, it is simple and can be easily implemented for such high dynamic optimization tasks, especially where a set of optimization parameters, for example, the number of resonators used in a final application, is unknown in advance.

CONCLUSION

In summary, we have reported a highly efficient and rather simple approach to design all-dielectric metasurfaces for nonlinear wavefront control. By encoding the third harmonic phase and amplitude in a silicon nanodisk and employing MC simulation for amplitude optimization in combination with a sampling method for the selection of appropriate nanodisks, we have demonstrated the full nonlinear $0-2\pi$ phase control with high and truly uniform amplitude. The robustness of our approach has been proved by designing TH beam deflectors in the optical range. We theoretically achieved the TH beam deflection into the desired channel with an average peak power-independent conversion efficiency of 1.2×10^{-1} W^{-2} that is the record value for silicon metasurfaces reported so far, to the best of our knowledge. The diffraction efficiency of the metadeflectors has been found to depend on the lattice period, gaps between resonators as well as whether they operate off- or on-resonance and can be increased by including additional far-field quantities in the optimization process. We expect that the proposed approach will be widely applied as alternative to more complex optimization algorithms for the design and optimization of metasurfaces for diverse beam-shaping applications.

METHODS

All numerical simulations were performed using COMSOL Multiphysics which employs a finite element method in frequency domain for the calculation of electromagnetic fields.[48] Our simulation model for the design and optimization step is reduced to a unit cell with a single resonator from the entire structure of the metasurface (see Figure 1b). The surface character of the structure is maintained by applying Floquet periodic boundary conditions to the unit cell in the x- and y-directions to imitate an infinite surface of identical resonators. The boundaries in the z-direction are set to open boundary conditions by adding perfectly matched layers (PML) in order to absorb the outgoing electromagnetic waves. Additionally, the model contains lossless integration ports above and below the resonator where the different far-field quantities at the FF and TH are calculated by a near-field to far-field transformation (NFFFT) for periodic structures as[50]

$$\boldsymbol{E}_{\text{far-field},m,n}(\omega) = \frac{1}{A_p}\int_0^{x_p}\int_0^{y_p} \boldsymbol{E}(\omega, x, y, z_0)\exp(jk_{x,m}x)\exp(jk_{y,n}y)\mathrm{d}y\ \mathrm{d}x \tag{1}$$

where $k_{x,m} = \frac{2\pi m}{x_p}$ and $k_{y,n} = \frac{2\pi n}{y_p}$ are periodicity wave numbers, $A_p = x_p y_p$ is the cross-section area of the unit cell. These ports are set to be located in the radiative near-field region of the resonator, in which the evanescent part of the emitted fields is sufficiently small. The nonlinear radiation is calculated via a two steps simulation approach employing an undepleted pump approximation in which the back coupling of the generated TH on the fundamental excitation signal is assumed to be negligible. In the first step, the periodic unit cell with the resonator is excited from the air side with a linear x-polarized plane wave propagating in the negative z-direction at the fundamental frequency ω. We use a pump wavelength of 1615 nm with input power density of 1 GW cm^{-2}. Then, the resulting local electric field and nonlinear polarization induced inside the resonator are calculated. The third-order nonlinear polarization of silicon at frequency 3ω is calculated as $\boldsymbol{P}_{\mathbf{NL}}^{(3)}(3\omega, \boldsymbol{r}) = \varepsilon_0\chi^{(3)}(\boldsymbol{E}(\omega, \boldsymbol{r})\cdot\boldsymbol{E}(\omega, \boldsymbol{r}))\boldsymbol{E}(\omega, \boldsymbol{r})$, where the third-order susceptibility tensor $\chi^{(3)}$ is considered as isotropic with a constant value of 2.45×10^{-19} m^2/V^2.[52] In the second step, the locally generated nonlinear currents inside the resonator $\boldsymbol{J}_{\text{ext}}(3\omega, \boldsymbol{r}) = j3\omega\boldsymbol{P}_{\mathbf{NL}}^{(3)}(3\omega, \boldsymbol{r})$ are injected as local current sources in a second simulation run. Subsequently, the generated phase and amplitude of the TH field in the zero-diffracted order ($k_x = k_y = 0$) in the transmission direction are calculated using eq 1. The calculation of electromagnetic fields generated by the supercell composed of several resonators are performed in similar way. All calculations use the refractive index of crystalline silicon from the measured dispersion curve.[53] The refractive index of SiO_2 substrate at fundamental and third harmonic frequency is set to $n_s = 1.44$ and 1.46, respectively.

ASSOCIATED CONTENT

Supporting Information

The Supporting Information is available free of charge at https://pubs.acs.org/doi/10.1021/acsphotonics.2c01967.

Analysis of the origin of the enhanced TH emission in optimum set 3 of high intensity used for nonlinear beam steering; electric near-fields generated by the designed supercells, and calculation of averaged conversion efficiencies (PDF)

AUTHOR INFORMATION

Corresponding Authors

Jens Förstner − *Paderborn University, Theoretical Electrical Engineering, 33098 Paderborn, Germany;* orcid.org/0000-0001-7059-9862; Email: jens.foerstner@uni-paderborn.de

https://doi.org/10.1021/acsphotonics.2c01967
ACS Photonics XXXX, XXX, XXX−XXX

Viktor Myroshnychenko − *Paderborn University, Theoretical Electrical Engineering, 33098 Paderborn, Germany;* orcid.org/0000-0001-6431-746X; Email: viktor.myroshnychenko@gmail.com

Author

David Hähnel − *Paderborn University, Theoretical Electrical Engineering, 33098 Paderborn, Germany*

Complete contact information is available at: https://pubs.acs.org/10.1021/acsphotonics.2c01967

Funding

The authors gratefully acknowledge financial support from the Deutsche Forschungsgemeinschaft (DFG) via TRR142, project number 231447078, subprojects C05 and B06.

Notes

The authors declare no competing financial interest.

■ ACKNOWLEDGMENTS

The authors acknowledge computing time support provided by the Paderborn Center for Parallel Computing (PC^2). V. Myroshnychenko also thanks S. Kruk for fruitful discussions.

■ REFERENCES

(1) Chen, S.; Li, Z.; Zhang, Y.; Cheng, H.; Tian, J. Phase manipulation of electromagnetic waves with metasurfaces and its applications in nanophotonics. *Advanced Optical Materials* **2018**, *6*, 1800104.

(2) Zhang, S.; Wong, C. L.; Zeng, S.; Bi, R.; Tai, K.; Dholakia, K.; Olivo, M. Metasurfaces for biomedical applications: imaging and sensing from a nanophotonics perspective. *Nanophotonics* **2020**, *10*, 259−293.

(3) Paniagua-Domínguez, R.; Ha, S. T.; Kuznetsov, A. I. Active and tunable nanophotonics with dielectric nanoantennas. *Proceedings of the IEEE* **2020**, *108*, 749−771.

(4) Pertsch, T.; Kivshar, Y. Nonlinear optics with resonant metasurfaces. *MRS Bull.* **2020**, *45*, 210−220.

(5) Solntsev, A. S.; Agarwal, G. S.; Kivshar, Y. S. Metasurfaces for quantum photonics. *Nat. Photonics* **2021**, *15*, 327−336.

(6) Yu, N.; Aieta, F.; Genevet, P.; Kats, M. A.; Gaburro, Z.; Capasso, F. A broadband, background-free quarter-wave plate based on plasmonic metasurfaces. *Nano Lett.* **2012**, *12*, 6328−6333.

(7) Abouelatta, M. A.; Hameed, M. F. O.; Obayya, S. Highly efficient ultrathin broadband quarter-waveplate based on plasmonic metasurface. *Optik* **2021**, *239*, 166770.

(8) Kruk, S.; Hopkins, B.; Kravchenko, I. I.; Miroshnichenko, A.; Neshev, D. N.; Kivshar, Y. S. Invited article: Broadband highly efficient dielectric metadevices for polarization control. *APL Photonics* **2016**, *1*, 030801.

(9) Guo, Q.; Zhu, H.; Liu, F.; Zhu, A. Y.; Reed, J. C.; Yi, F.; Cubukcu, E. Silicon-on-glass graphene-functionalized leaky cavity mode nanophotonic biosensor. *ACS Photonics* **2014**, *1*, 221−227.

(10) Guo, Q.; Shi, Z.; Huang, Y.-W.; Alexander, E.; Qiu, C.-W.; Capasso, F.; Zickler, T. Compact single-shot metalens depth sensors inspired by eyes of jumping spiders. *Proc. Natl. Acad. Sci. U. S. A.* **2019**, *116*, 22959−22965.

(11) Aieta, F.; Genevet, P.; Kats, M. A.; Yu, N.; Blanchard, R.; Gaburro, Z.; Capasso, F. Aberration-free ultrathin flat lenses and axicons at telecom wavelengths based on plasmonic metasurfaces. *Nano Lett.* **2012**, *12*, 4932−4936.

(12) Aieta, F.; Kats, M. A.; Genevet, P.; Capasso, F. Multiwavelength achromatic metasurfaces by dispersive phase compensation. *Science* **2015**, *347*, 1342−1345.

(13) Almeida, E.; Bitton, O.; Prior, Y. Nonlinear metamaterials for holography. *Nat. Commun.* **2016**, *7*, 12533.

(14) Huang, L.; Chen, X.; Mühlenbernd, H.; Zhang, H.; Chen, S.; Bai, B.; Tan, Q.; Jin, G.; Cheah, K.-W.; Qiu, C.-W.; Li, J.; Zentgraf, T.; Zhang, S. Three-dimensional optical holography using a plasmonic metasurface. *Nat. Commun.* **2013**, *4*, 2808.

(15) Wang, L.; Kruk, S.; Tang, H.; Li, T.; Kravchenko, I.; Neshev, D. N.; Kivshar, Y. S. Grayscale transparent metasurface holograms. *Optica* **2016**, *3*, 1504−1505.

(16) Balthasar Mueller, J. P.; Rubin, N. A.; Devlin, R. C.; Groever, B.; Capasso, F. Metasurface polarization optics: independent phase control of arbitrary orthogonal states of polarization. *Phys. Rev. Lett.* **2017**, *118*, 113901.

(17) Ahmed, H.; Rahim, A. A.; Maab, H.; Ali, M. M.; Mahmood, N.; Naureen, S. Phase engineering with all-dielectric metasurfaces for focused-optical-vortex (FOV) beams with high cross-polarization efficiency. *Opt. Mater. Express* **2020**, *10*, 434−448.

(18) Frese, D.; Wei, Q.; Wang, Y.; Cinchetti, M.; Huang, L.; Zentgraf, T. Nonlinear bicolor holography using plasmonic metasurfaces. *ACS Photonics* **2021**, *8*, 1013−1019.

(19) Liu, B.; Sain, B.; Reineke, B.; Zhao, R.; Meier, C.; Huang, L.; Jiang, Y.; Zentgraf, T. Nonlinear wavefront control by geometric-phase dielectric metasurfaces: influence of mode field and rotational symmetry. *Advanced Optical Materials* **2020**, *8*, 1902050.

(20) Staude, I.; Miroshnichenko, A. E.; Decker, M.; Fofang, N. T.; Liu, S.; Gonzales, E.; Dominguez, J.; Luk, T. S.; Neshev, D. N.; Brener, I.; Kivshar, Y. Tailoring directional scattering through magnetic and electric resonances in subwavelength silicon nanodisks. *ACS Nano* **2013**, *7*, 7824−7832.

(21) Aoni, R. A.; Rahmani, M.; Xu, L.; Zangeneh Kamali, K.; Komar, A.; Yan, J.; Neshev, D.; Miroshnichenko, A. E. High-efficiency visible light manipulation using dielectric metasurfaces. *Sci. Rep.* **2019**, *9*, 6510.

(22) Kepič, P.; Ligmajer, F.; Hrtoň, M.; Ren, H.; Menezes, L. d. S.; Maier, S. A.; Šikola, T. Optically tunable Mie resonance VO2 nanoantennas for metasurfaces in the visible. *ACS Photonics* **2021**, *8*, 1048−1057.

(23) Wang, L.; Kruk, S.; Koshelev, K.; Kravchenko, I.; Luther-Davies, B.; Kivshar, Y. Nonlinear wavefront control with all-dielectric metasurfaces. *Nano Lett.* **2018**, *18*, 3978−3984.

(24) Myroshnychenko, V.; Rodríguez-Fernández, J.; Pastoriza-Santos, I.; Funston, A. M.; Novo, C.; Mulvaney, P.; Liz-Marzán, L. M.; García de Abajo, F. J. Modelling the optical response of gold nanoparticles. *Chem. Soc. Rev.* **2008**, *37*, 1792−1805.

(25) Asenjo-Garcia, A.; Manjavacas, A.; Myroshnychenko, V.; Garcia de Abajo, F. J. Magnetic polarization in the optical absorption of metallic nanoparticles. *Opt. Express* **2012**, *20*, 28142−28152.

(26) Krasnok, A.; Tymchenko, M.; Alù, A. Nonlinear metasurfaces: a paradigm shift in nonlinear optics. *Mater. Today* **2018**, *21*, 8−21.

(27) Li, G.; Zhang, S.; Zentgraf, T. Nonlinear photonic metasurfaces. *Nature Reviews Materials* **2017**, *2*, 17010.

(28) Chen, S.; Li, G.; Cheah, K. W.; Zentgraf, T.; Zhang, S. Controlling the phase of optical nonlinearity with plasmonic metasurfaces. *Nanophotonics* **2018**, *7*, 1013−1024.

(29) Grinblat, G. Nonlinear dielectric nanoantennas and metasurfaces: Frequency conversion and wavefront control. *ACS Photonics* **2021**, *8*, 3406−3432.

(30) Gao, Y.; Fan, Y.; Wang, Y.; Yang, W.; Song, Q.; Xiao, S. Nonlinear holographic all-dielectric metasurfaces. *Nano Lett.* **2018**, *18*, 8054−8061.

(31) Schlickriede, C.; Kruk, S. S.; Wang, L.; Sain, B.; Kivshar, Y.; Zentgraf, T. Nonlinear imaging with all-dielectric metasurfaces. *Nano Lett.* **2020**, *20*, 4370−4376.

(32) Kruk, S. S.; Wang, L.; Sain, B.; Dong, Z.; Yang, J.; Zentgraf, T.; Kivshar, Y. Asymmetric parametric generation of images with nonlinear dielectric metasurfaces. *Nat. Photonics* **2022**, *16*, 561−565.

(33) Grinblat, G.; Zhang, H.; Nielsen, M. P.; Krivitsky, L.; Berté, R.; Li, Y.; Tilmann, B.; Cortés, E.; Oulton, R. F.; Kuznetsov, A. I.; Maier, S. A. Efficient ultrafast all-optical modulation in a nonlinear crystalline gallium phosphide nanodisk at the anapole excitation. *Science Advances* **2020**, *6*, No. eabb3123.

(34) Celebrano, M.; Wu, X.; Baselli, M.; Großmann, S.; Biagioni, P.; Locatelli, A.; De Angelis, C.; Cerullo, G.; Osellame, R.; Hecht, B.; Duò, L.; Ciccacci, F.; Finazzi, M. Mode matching in multiresonant plasmonic nanoantennas for enhanced second harmonic generation. *Nat. Nanotechnol.* **2015**, *10*, 412−417.
(35) Huttunen, M. J.; Reshef, O.; Stolt, T.; Dolgaleva, K.; Boyd, R. W.; Kauranen, M. Efficient nonlinear metasurfaces by using multiresonant high-Q plasmonic arrays. *J. Opt. Soc. Am. B* **2019**, *36*, E30−E35.
(36) Shcherbakov, M. R.; Neshev, D. N.; Hopkins, B.; Shorokhov, A. S.; Staude, I.; Melik-Gaykazyan, E. V.; Decker, M.; Ezhov, A. A.; Miroshnichenko, A. E.; Brener, I.; Fedyanin, A. A.; Kivshar, Y. S. Enhanced third-harmonic generation in silicon nanoparticles driven by magnetic response. *Nano Lett.* **2014**, *14*, 6488−6492.
(37) Grinblat, G.; Li, Y.; Nielsen, M. P.; Oulton, R. F.; Maier, S. A. Degenerate four-wave mixing in a multiresonant germanium nanodisk. *ACS Photonics* **2017**, *4*, 2144−2149.
(38) Mansouree, M.; Arbabi, A. Metasurface design using level-set and gradient descent optimization techniques. *2019 International Applied Computational Electromagnetics Society Symposium (ACES)*; ACES, 2019; pp 1−2.
(39) Deng, Y.; Korvink, J. G. Topology optimization for three-dimensional electromagnetic waves using an edge element-based finite-element method. *Proceedings of the Royal Society A: Mathematical, Physical and Engineering Sciences* **2016**, *472*, 20150835.
(40) Sell, D.; Yang, J.; Doshay, S.; Fan, J. A. Periodic dielectric metasurfaces with high-efficiency, multiwavelength functionalities. *Advanced Optical Materials* **2017**, *5*, 1700645.
(41) Phan, T.; Sell, D.; Wang, E. W.; Doshay, S.; Edee, K.; Yang, J.; Fan, J. A. High-efficiency, large-area, topology-optimized metasurfaces. *Light: Science & Applications* **2019**, *8*, 48.
(42) Huntington, M. D.; Lauhon, L. J.; Odom, T. W. Subwavelength lattice optics by evolutionary design. *Nano Lett.* **2014**, *14*, 7195−7200.
(43) Wiecha, P. R.; Arbouet, A.; Girard, C.; Lecestre, A.; Larrieu, G.; Paillard, V. Evolutionary multi-objective optimization of colour pixels based on dielectric nanoantennas. *Nat. Nanotechnol.* **2017**, *12*, 163−169.
(44) Malkiel, I.; Mrejen, M.; Nagler, A.; Arieli, U.; Wolf, L.; Suchowski, H. Plasmonic nanostructure design and characterization via Deep Learning. *Light: Science & Applications* **2018**, *7*, 60.
(45) Liu, Z.; Zhu, D.; Rodrigues, S. P.; Lee, K.-T.; Cai, W. Generative model for the inverse design of metasurfaces. *Nano Lett.* **2018**, *18*, 6570−6576.
(46) Kudyshev, Z. A.; Kildishev, A. V.; Shalaev, V. M.; Boltasseva, A. Machine-learning-assisted metasurface design for high-efficiency thermal emitter optimization. *Applied Physics Reviews* **2020**, *7*, 021407.
(47) Gigli, C.; Li, Q.; Chavel, P.; Leo, G.; Brongersma, M. L.; Lalanne, P. Fundamental limitations of Huygens' metasurfaces for optical beam shaping. *Laser & Photonics Reviews* **2021**, *15*, 2000448.
(48) COMSOL Multiphysics; COMSOL AB, Stockholm, Sweden, www.comsol.com (accessed 2023−05−03).
(49) Gigli, C.; Marino, G.; Artioli, A.; Rocco, D.; De Angelis, C.; Claudon, J.; Gerard, J.-M.; Leo, G. Tensorial phase control in nonlinear meta-optics. *Optica* **2021**, *8*, 269−276.
(50) Taflove, A.; Hagness, S. *Computational Electrodynamics: The Finite-Difference Time-Domain Method*, 3rd ed.; 2005; Vol. *2062*.
(51) Swanson, G. J. Binary optics technology: theoretical limits on the diffraction efficiency of multilevel diffractive optical elements. *Technical report*; Lincoln Laboratory, Massachusetts Institute of Technology, 1991.
(52) Hon, N. K.; Soref, R.; Jalali, B. The third-order nonlinear optical coefficients of Si, Ge, and $Si_{1-x}Ge_x$ in the midwave and longwave infrared. *J. Appl. Phys.* **2011**, *110*, 011301.
(53) Green, M. A. Self-consistent optical parameters of intrinsic silicon at 300K including temperature coefficients. *Sol. Energy Mater. Sol. Cells* **2008**, *92*, 1305−1310.

https://doi.org/10.1021/acsphotonics.2c01967
ACS Photonics XXXX, XXX, XXX−XXX